Review of Scientific Instruments ARTICLE scitation.org/journal/rsi

A high performance active noise control system for magnetic fields

Cite as: Rev. Sci. Instrum. 92, 124702 (2021); doi: 10.1063/5.0062650
Submitted: 7 July 2021 • Accepted: 8 November 2021 •
Published Online: 3 December 2021

Tadas Pyragius[a] and Kasper Jensen[a]

AFFILIATIONS

School of Physics and Astronomy, University of Nottingham, University Park, Nottingham NG7 2RD, United Kingdom

[a]Authors to whom correspondence should be addressed: t.pyragius@gmail.com and kasper.jensen@nottingham.ac.uk

ABSTRACT

We present a system for active noise control of environmental magnetic fields based on a filtered-x least mean squares algorithm. The system consists of a sensor that detects the ambient field noise and an error sensor that measures the signal of interest contaminated with the noise. These signals are fed to an adaptive algorithm that constructs a physical anti-noise signal canceling the local magnetic field noise. The proposed system achieves a maximum of 35 dB root-mean-square noise suppression in the DC-1 kHz band and 55 and 50 dB amplitude suppression of 50 and 150 Hz AC line noise, respectively, for all three axial directions of the magnetic vector field.

I. INTRODUCTION

Magnetically low noise environments are important across many metrologically relevant areas ranging from medical imaging of biomagnetic fields from the heart and brain to non-destructive evaluation of car batteries.[1–5] Currently, optically pumped magnetometers (OPMs) are state of the art magnetic field sensors and are a promising alternative to conventional superconducting quantum interference device (SQUID) and fluxgate magnetometers in both shielded and unshielded conditions.[6–10] A wider adoption of quantum magnetometers for ultra-low field precision measurements has been limited to magnetically shielded environments due to large external magnetic field noise, making such setups expensive. Conventionally, partial magnetic field noise cancellation is achieved via a combination of proportional-integral-derivative (PID) controllers that are sometimes combined with a feed-forward system.[11–15] While these systems are effective in field noise compensation and control, they require extensive hands on tuning, which is heavily dependent on the implemented hardware constraints. As a result, the tuning parameters cannot be easily transferred from one system to another. Furthermore, the performance of the noise suppression can be additionally limited by hardware and processing delays and system imperfections, which often cannot be compensated for. In cases where the focus is on unwanted periodic environmental noise signals, e.g., from rotating machinery, adaptive approaches have been implemented.[16] However, as before, some of these methods require extensive manual tuning of the filter coefficients as well as limiting the compensation to fixed AC noise frequency signals. Finally, it is often the case that the noise environment and the transfer function of the system are not known in advance or cannot be adequately modeled, rendering these methodologies unable to cope.

In this work, we demonstrate how these technical issues can be overcome using an active magnetic field compensation method based on adaptive filtering. Active noise control (ANC) is achieved by introducing a canceling "anti-noise" signal through a secondary source. The secondary source is driven by an electronic system that utilizes a specific signal processing algorithm (such as an adaptive algorithm) for the particular cancellation scheme (see Fig. 1). This technique is widely exploited in noise canceling headphone technology, vibration control, and exhaust ducts in ventilation and cooling systems.[17–20] While adaptive filtering techniques have been demonstrated in unwanted noise cancellation of electric and magnetic fields in the context of electrocardiography (ECG) and magnetocardiography (MCG), the noise cancellation was performed on the acquired data.[21,22] This process is known as adaptive noise cancellation.[23] In contrast, active noise control (ANC) generates a physical anti-noise signal.[16,20] In our implementation (see Fig. 2), the three components of the magnetic field are measured using three-axis fluxgate magnetometers (Bartington MAG690), and the magnetic field is actively controlled using a three-axis square Helmholtz coil system in order to create a magnetically quiet environment in the center of the coil

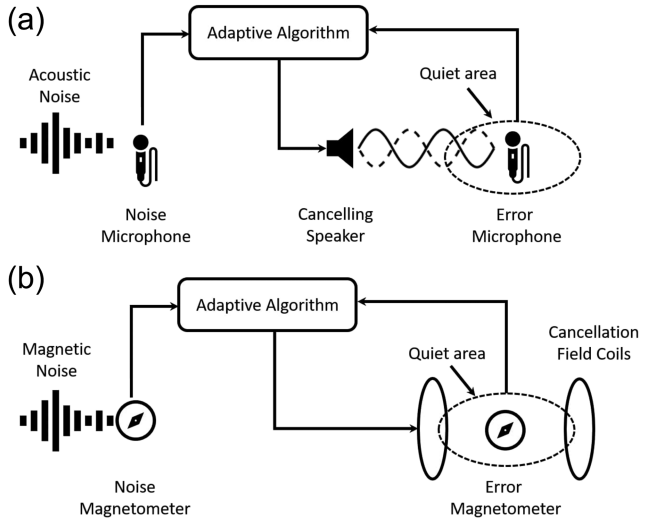

FIG. 1. (a) Basic implementation of active noise control in the acoustic domain. Here, a noise reference microphone listens to unwanted environmental noise and feeds that information to the adaptive algorithm. The adaptive algorithm then calculates the anti-noise signal and outputs it through a noise canceling speaker. The error microphone measures the noise + anti-noise signal and feeds it back to the adaptive algorithm for adjustment if necessary. (b) Analogous implementation of active noise control in the magnetic field domain. Here, the microphones are replaced with field sensitive magnetometers and the compensation is achieved by magnetic field coils.

system. Active noise control has a number of advantages over adaptive noise cancellation techniques. First, the noise signals in the environment are typically orders of magnitude larger than the signals of interest (e.g., magnetocardiography signals in the pT range compared to the 50 Hz line noise in nT). This results in the requirement for a larger dynamic range which reduces the signal resolution of the signals of interest due to the limited number of bits in the analog-to-digital conversion (ADC). The ANC system cancels the physical noise signals, which enables one to reduce the analog input range for the same number of bits, thus increasing the signal resolution and reducing the noise floor. In the context of OPMs [in particular, spin-exchange relaxation-free (SERF) OPMs], one of the key feature that determines the sensitivity of an OPM is its intrinsic linewidth.[24] When the environmental noise (e.g., 50 Hz noise) is larger than the OPM linewidth, this broadens the linewidth and

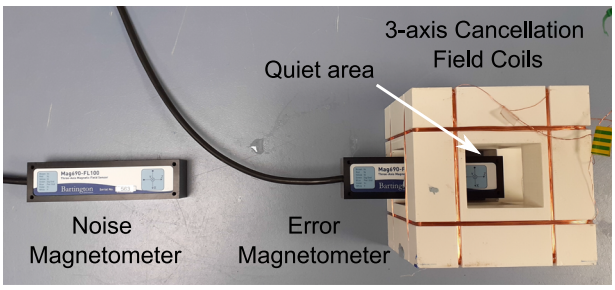

FIG. 2. Picture of the experimental setup.

reduces the sensitivity. ANC reduces the ambient magnetic field noise which in turn reduces the OPM linewidth increasing its sensitivity, thus enabling its operation in otherwise environmentally noisy conditions. This has additional implications in gradiometric magnetic field measurements using OPMs where the performance relies on the high common-mode-noise-rejection ratio (CMMR).[25] Since the ANC relies on canceling common-mode noise, the gradiometric technique would benefit from a further increase in CMMR, thus enabling enhanced field sensitivity. The ANC approach may also improve the field stability in areas where it is paramount, for example, extracting and resolving narrow line magnetic resonances in nuclear magnetic resonance (NMR) or improving image contrast in magnetic resonance imaging (MRI). We also note that active noise cancellation using a self-adaptive scheme with a single OPM has recently been implemented.[26]

This paper is organized as follows: Secs. II and III walk through the motivation and process of secondary path modeling and its application to anti-noise generation via the Filtered-x Least Mean Squares (FxLMS) algorithm. Section IV contains the results and discussion of the active noise control system for magnetic field noise cancellation, its scope, limitations, and potential improvements. Section V sets out the conclusion.

II. SECONDARY PATH MODELLING

Due to the complexity of adaptive filters, they cannot be trivially implemented on analog electronic platforms. As a result, adaptive filter technology is usually deployed on digital platforms such as application specific integrated circuits (ASICs) acting as digital signal processing (DSP) chips or field-programmable gate arrays (FPGAs). These digital platforms deal with discrete signals and thus require the mathematical formalism of discrete time signals. The mathematical details have been widely and extensively discussed on the textbook level and can be found in Ref. 27.

For a broadband ANC system, the first stage of implementation consists of modeling the secondary path [see Fig. 3(a)]. The secondary path takes into account the hardware effects of the output for a given input signal. The generated signal is detected by a sensor with a transfer function that modifies the measured signal. This signal is then propagated through the system that further modifies the signal. We want to compensate for these secondary path effects. This requires one to estimate the approximate secondary path response, i.e., we want to find a filter coefficient transfer function that can effectively approximate the transfer function of the secondary path, i.e., $C(z) \approx H(z)$, which corresponds to discrete transfer functions of the estimated and actual secondary paths, respectively. Here, we have used the z-transform formalism to define the transfer functions. To do this, we generate a white noise signal, $y(n)$, that satisfies

$$\mathrm{E}[y(n)] = 0, \tag{1}$$

$$\mathrm{Var}[y(n)] = \sigma^2, \tag{2}$$

$$\mathrm{E}[y(n) * y(n-k)] = 0, \quad \forall\, k \in \mathbb{Z}^+, \tag{3}$$

where E is the expectation value, Var is the variance with a value σ^2, and the last term is the auto-correlation between the two time

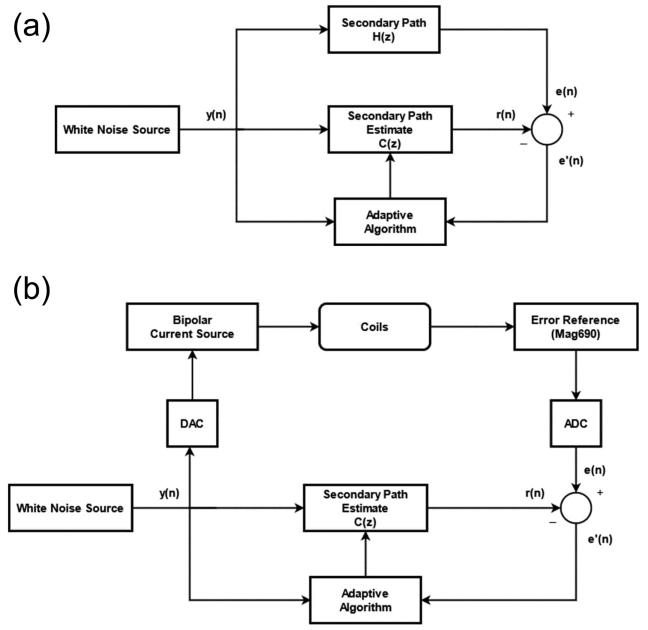

FIG. 3. (a) Theoretical structure of the secondary path $H(z)$. (b) Experimental structure of the secondary path in the context of magnetic field generation and measurement. Here, the white noise signal is fed to the digital-to-analog converter (DAC) driving a bipolar current source (BCS) with uniform field coils. The same white noise signal is fed to the adaptive algorithm as a reference. An error reference magnetometer measures the generated white noise field which is then used to calculate the error signal and adjust the secondary path coefficients. Here, the secondary path $H(z)$ consists of a DAC, BCS, coils, magnetometers, and an ADC with an anti-aliasing filter (not shown).

delayed white noise signals. The white noise signal is fed to a bipolar current source that drives a pair of Helmholtz coils. Simultaneously, we use the generated $y(n)$ white noise as a reference for the secondary path estimate filter $C(z)$ and the least-mean-squares (LMS) adaptive algorithm. The generated white noise magnetic field is sensed by a fluxgate magnetometer (Bartington Mag690), and then an anti-aliasing filter is fed into an analog-to-digital converter. The sensed magnetic field corresponds to our secondary path response $e(n)$. For the adaptive model, the computed response $r(n)$ is given by

$$r(n) = \sum_{i=0}^{M-1} c_i(n) y(n-i), \tag{4}$$

where n is the discrete time increment index, $c_i(n)$ is the ith filter coefficient of the discrete transfer function of the estimated secondary path $C(z)$ (equivalent to an adaptive filter), and M is the total number of taps in the adaptive filter. The number of filter taps relates to the frequency resolution of the filter by $f_{\text{res}} = f_s/M$, where f_s is the sampling rate. The coefficients of the adaptive finite-impulse response (FIR) filter $c_i(n)$ are the quantized values of the impulse response of the frequency transfer function.[28] We followed a standard convention and chose our adaptive filter to be a finite-impulse response (FIR) filter.[20] Adaptive filtering can be implemented using infinite-impulse response (IIR) filters as well. However, there are several reasons why we chose the implementation of FIR filters over the IIR ones. First, unlike IIR filters, the FIR filters are bounded due to having a finite number of filter coefficients over recursive IIR. This makes the output of the FIR filter inherently stable, which cannot be guaranteed using IIR filters. Second, IIR filters have a slower rate of convergence for the adaptive algorithm than FIR filters, which can result in adaptive stalling resulting in the poor performance of noise suppression. This issue is further exacerbated by the fact that the adaptation may not converge to a local minimum because the mean-square error function of adaptive IIR filters is generally non-quadratic.[20,29]

The computed response $r(n)$ of the adaptive filter is then compared with the measured response of the system $e(n)$, which allows us to compute the error $e'(n)$,

$$e'(n) = e(n) - r(n). \tag{5}$$

The measured error can then be used to update the filter coefficients of the secondary path estimate $C(z)$,

$$c_i(n+1) = c_i(n) + \mu_{\text{sp}} e'(n) y(n-i), \tag{6}$$

where μ_{sp} is the step size of the update during secondary path modeling and must satisfy[16]

$$0 < \mu_{\text{sp}} < \frac{1}{MP_y}, \tag{7}$$

where P_y is the power of the signal $y(n)$. With the updated values of the coefficients $c_i(n)$ and a new secondary path estimate $C(z)$, the procedure is repeated iteratively to compute the new error value and update the corresponding coefficients. After some time, the iterative procedure is stopped. The final computed secondary path coefficients $c(i)$ and the estimated secondary path are used in the next stage of active noise control using the FxLMS algorithm.

III. FILTERED LEAST MEAN SQUARES (FxLMS) ALGORITHM

With the estimated effect of the secondary path, the next stage involves actively compensating for the noise. A reference noise signal $x(n)$ is propagated through the estimated secondary path $C(z)$, which yields the filtered version of the reference noise signal,

$$x'(n) = \sum_{i=0}^{M-1} c(i) x(n-i). \tag{8}$$

We then proceed to compute the anti-noise signal,

$$y(n) = \sum_{i=0}^{M-1} w_i(n) x(n-i), \tag{9}$$

where $w_i(n)$ is the ith coefficient of the adaptive filter $W(z)$. The adaptive coefficients are then updated according to

$$w_i(n+1) = w_i(n) - \mu_{\text{anc}} e(n) x'(n-i), \tag{10}$$

where $e(n)$ is the error reference signal and μ_{anc} is the ANC filter update step size, where typically $\mu_{\text{sp}} \neq \mu_{\text{anc}}$. The procedure is repeated. See Fig. 4 for schematic details.

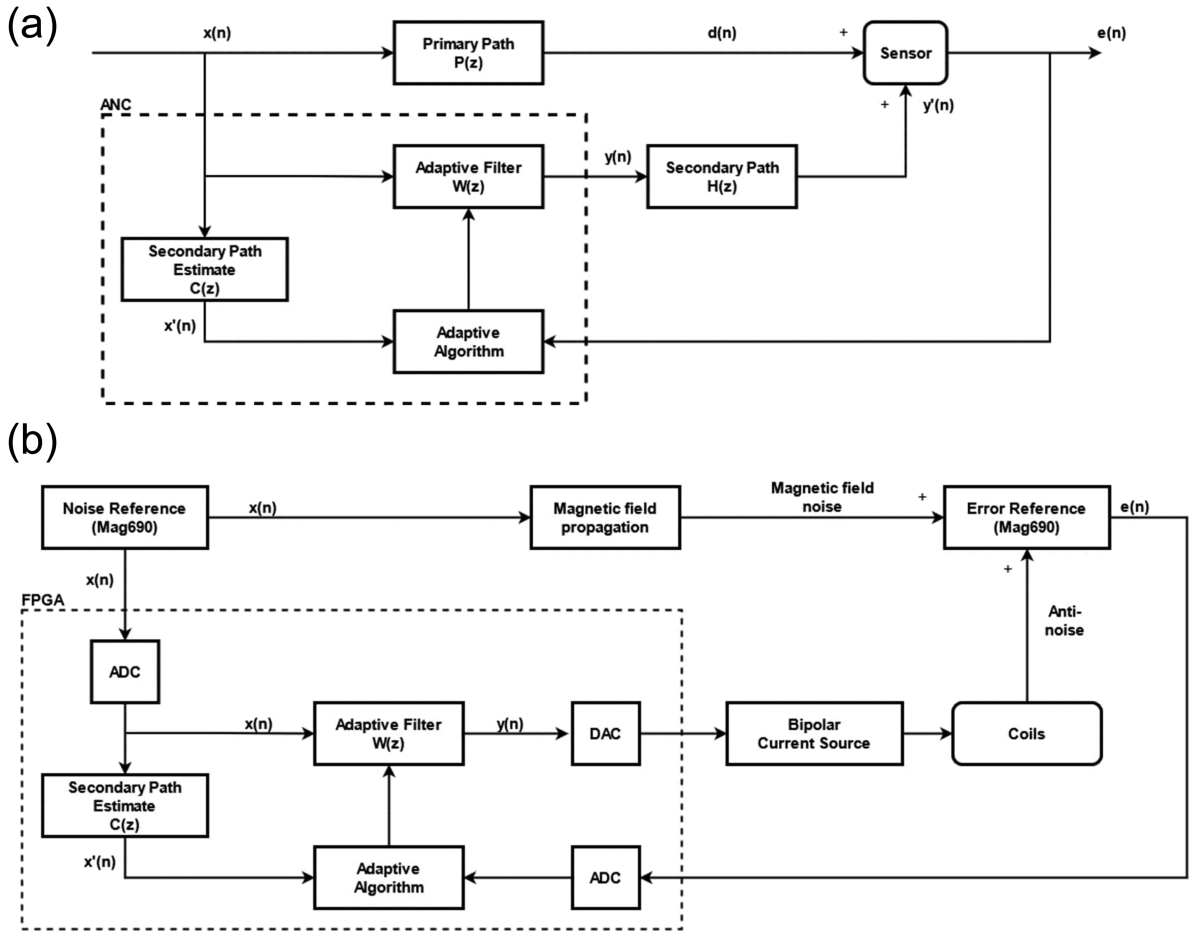

FIG. 4. (a) Theoretical structure of the primary and secondary paths. The ANC box contains the algorithmic elements of the adaptive filter that generates an anti-noise signal. Here, we assume that the primary path $P(z)$ transfer function does not have an appreciable effect on the signal detected at the sensor. (b) Experimental structure of the primary and secondary paths in the context of magnetic field generation and measurement. The ANC algorithm is contained within the FPGA chip.

IV. EXPERIMENTAL IMPLEMENTATION

A. Outline of the ANC procedure

Applications of active noise control in noise canceling systems generally deal with AC coupled signals (e.g., acoustic or vibration signals). This becomes problematic when a signal acquires a DC component, which is the case in ANC applications of magnetic field cancellation due to the Earth's field component. A DC component affects the secondary path analysis by biasing the filter coefficients that render the cancellation system ineffective. As a result, in order to obtain a good estimate for the secondary path, $C(z)$, one must cancel the DC component of the ambient magnetic field and only then proceed with the online secondary path estimation. This step is achieved by a PID controller that prestabilizes the magnetic field around zero. The output voltage sent to the bipolar current source that approximately cancels the Earth's field is then used as a DC control during the secondary path analysis combined with the white noise reference signal for impulse response modeling with the PID switched off. This ensures that the generated magnetic field signals are centered around zero without any DC offset. The secondary path modeling is run sequentially for each magnetic field vector axis individually for a given duration T_{sp} and a step size μ_{sp}. The estimated secondary path coefficients are then used to construct a secondary path response filter that enables the FxLMS algorithm to calculate the anti-noise signal in active noise control. The algorithm is deployed on NI's sbRIO-9627 FPGA and controlled using LabVIEW with NI's proprietary adaptive filter toolkit.[30]

B. Secondary path estimation

The secondary path estimation follows an experimental setup depicted in Fig. 3(b). A band limited white noise signal is generated within the FPGA architecture and is used to drive a bipolar current source with a pair of Helmholtz coils producing a uniform white noise magnetic field around zero. The generated magnetic field is sensed by the error reference fluxgate magnetometer, which is then fed into the LMS algorithm on the FPGA to compute the error and

adjust the filter coefficients that attempt to minimize the error. The filter coefficients allow one to construct an estimate of the impulse response of the secondary path (see Fig. 5 for results). The profile of the secondary path impulse response depends on a number of various physical properties of the system such as anti-aliasing filters used for the ADCs, transfer functions of the coils, bipolar current source, etc., as well as the relative gains of the input and output signals. In our experimental setup, the three-axis system has identical hardware and software implementation including the anti-aliasing filters and the coils (near identical resistance, inductance, and number of turns). Consequently, the estimated secondary paths using the same experimental parameters are to a good approximation equivalent.

C. Active noise control using the FxLMS algorithm

The experimental layout of the FxLMS algorithm for active noise control is shown in Fig. 4(b). Here, the reference and error fluxgate magnetometers read the ambient and compensated magnetic fields that are fed to the FxLMS algorithm. The FxLMS algorithm compensates for the secondary path, adjusts the filter coefficients, and computes an anti-noise signal $y(n)$ [see Eqs. (8)–(10)], which drives the bipolar current source controlling a pair of Helmholtz coils to produce a uniform anti-noise magnetic field. The active noise control system is initialized sequentially for each magnetic field vector axis. Once the compensation reaches a steady state limit, the ANC system is disabled and the compensation is initialized for the next axis until a steady state is reached there and so on. Once each axial direction has converged with optimum filter coefficients, the ANC system is then switched on simultaneously for all three axial directions. In this configuration, the ANC algorithm is capable of compensating for AC as well as DC fields without requiring additional Earth's field nulling. The initial DC field nulling is only required during the secondary path estimation. Due to crosstalk between each axis direction, some field leakage occurs and the FxLMS algorithm has to re-adjust the optimum filter coefficients when operated in the three-axis mode. Figure 6(a) shows the time trace comparison between the ambient field noise with and without the ANC engaged with Figs. 7(a)–7(c), detailing the frequency band performance of ANC for each vector direction. As can be seen from Fig. 7, the ANC system is capable of almost completely suppressing the 50 Hz and its third harmonic, 150 Hz. This corresponds to 55 and 50 dB amplitude suppression with respect to the noise reference. Moreover, we find that the ANC performance is better than the conventional approach using a PID controller. Figure 7(b) shows the ANC performance for all three axial directions. One can observe from Fig. 7 that ANC is very effective in canceling the harmonic noise in the DC–1 kHz range with biggest noise reduction at lower frequencies. The noise performance is further broken down over different bandwidths (see Table I). Figure 7(c) shows the noise attenuation of noise for each frequency component. The attenuation in (dB) is given by the logarithm of the ratio of the measured ambient noise and the actively canceled noise,

$$\text{Attenuation } [\text{dB}] = 20\log_{10}\left(\frac{B_{\text{RMS noise ref.}}(f)}{B_{\text{RMS ANC comp.}}(f)}\right). \quad (11)$$

The 1 kHz bandwidth corresponds to the anti-aliasing terminated bandwidth of the analog acquisition that roughly corresponds to the bandwidth of the Mag690 fluxgate magnetometer. The maximum root-mean-square (rms) noise suppression is around 35 dB in the 1 kHz band. Commercial SERF OPMs have a typical bandwidth of 150 Hz and a dynamic range of ±5 nT and require an ambient magnetic field to be below 50 nT.[31] As seen in Table I, we achieve 3–7 nT rms noise in a 150 Hz bandwidth. With just a modest improvement of the performance of our ANC system, it would therefore be possible to operate a SERF OPM in unshielded conditions. We also note that the laboratory where the ANC system was deployed is exceptionally noisy due to high current experiments running in close proximity. In typical lab environments, the rms magnetic field noise is in the range of <100 nT.[14,15]

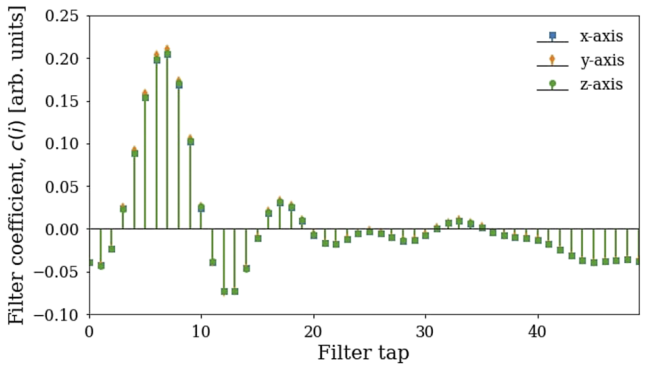

FIG. 5. Experimentally obtained secondary path estimates $C(z)$ for all three axial directions. Here, we have the finite-impulse response of a filter as a function of filter taps. The number of filter taps relates to the frequency resolution of the filter by $f_{\text{res}} = f_s/M$, where f_s is the sampling rate. We observe that the impulse response is shifted because the filter only operates on available samples with some additional delay. For an ideal low-pass filter, the filter coefficients follow a sinc function and the delay is given by $(M-1)/2f_s$. The secondary path consists of a DAC, a bipolar current source (BCS), a fluxgate (Mag690), an anti-aliasing low-pass (LP) filter, and an ADC. In this case, the specification for each hardware channel is the same, giving rise to identical secondary path coefficients.

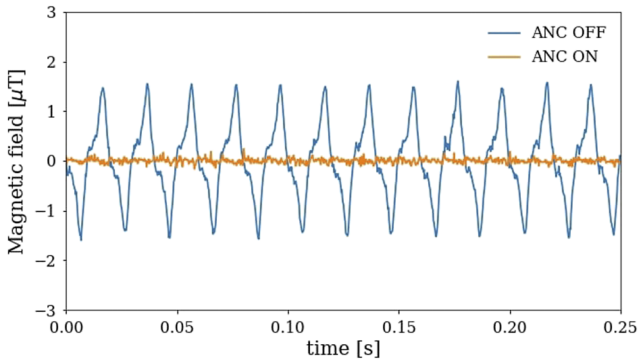

FIG. 6. Time trace of the error magnetometer signal before and after applying active noise control. The time trace for the ANC OFF case has been offset to subtract the DC Earth's field for visualization.

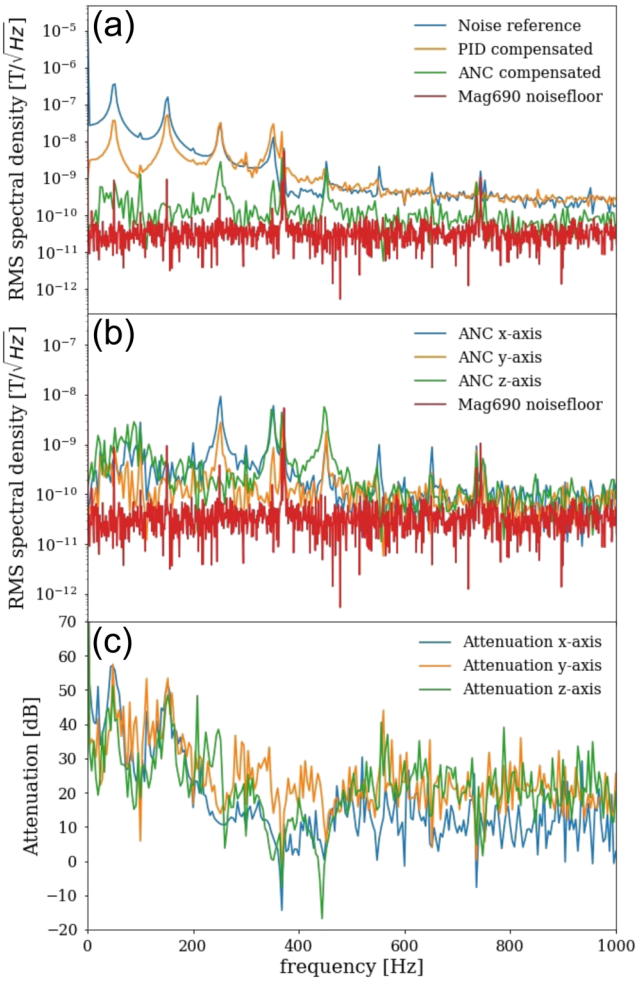

FIG. 7. (a) Root-mean-square amplitude spectral density of the magnetic field signals. The noise reference fluxgate monitors the ambient field environment. ANC compensated is the magnetic field measured by the error magnetometer, which monitors the canceled magnetic field noise. The PID compensated noise is the error magnetometer measuring the noise performance using the conventional proportional-integral-differential controller. (b) ANC performance rms amplitude spectral density for all three axial directions run simultaneously. The Mag690 noise floor is obtained inside a four-layer μ-metal shield in an open loop configuration. (c) ANC attenuation in dB for each axial direction with respect to the corresponding noise reference.

D. Performance limits and considerations

The performance of an FxLMS-based ANC system is limited by a number of factors. First, the control and sensing hardware imposes limits on the secondary path impulse response as well as the bandwidth. If the group delays introduced by the hardware are large, resulting in a long impulse response, the FxLMS algorithm will not be able to compensate well for the noise. This can be especially problematic if aggressive (high-order) anti-aliasing filters are used, which introduce long group delays. To circumvent this, a low order low-pass filter can be used. This, however, comes at the expense of having to increase the sampling rate (oversampling). This introduces further limitations due to the fact that there is an upper time limit of the processing speed of the FxLMS algorithm. Another way to counter the long delay response is to increase the filter length. However, this increases the processing time and resources on the FPGA hardware and reduces the maximum bandwidth. Moreover, while increasing the filter length reduces the steady state error, it degrades the rate of convergence process to reach the steady state error.[32]

TABLE I. rms noise performance of PID and ANC systems benchmarked against the environmental noise. The bottom table expresses the rms magnetic field noise converted to frequency using the gyromagnetic ratio of cesium, γ = 350 kHz/G. Cesium is a common atomic species used in OPMs. The frequency values on the axis row correspond to the bandwidths for which the noise performance is calculated for.

	Noise		PID		ANC	
Axis	1 kHz	150 Hz	1 kHz	150 Hz	1 kHz	150 Hz
x-axis	800 nT	N/A	112 nT	80 nT	16 nT	7 nT
y-axis	150 nT	N/A	35 nT	25 nT	7 nT	3 nT
z-axis	450 nT	N/A	23 nT	16 nT	12 nT	7 nT

	Noise		PID		ANC	
Axis	1 kHz	150 Hz	1 kHz	150 Hz	1 kHz	150 Hz
x-axis	2800 Hz	N/A	392 Hz	280 Hz	56 Hz	24.5 Hz
y-axis	525 Hz	N/A	123 Hz	87.5 Hz	24.5 Hz	10.5 Hz
z-axis	1580 Hz	N/A	80.5 Hz	56 Hz	42 Hz	24.5 Hz

Another highly crucial ingredient in determining the performance of the ANC system is the noise coherence. In real world environments, multiple magnetic field noise sources may be present. These will have their own magnetic field noise profiles of varying amplitude, spectral profile, and phase. Due to the principle of superposition and field decay, the resulting environmental noise will have spatial and temporal inhomogeneities. Moreover, if any conductive objects are present in the vicinity of the noise or error reference magnetometers, the time varying magnetic fields will induce eddy currents in the conductive objects, which will produce their own respective magnetic fields.[33] As a result, the relative position of the noise and error reference magnetic field sensors can have a significant effect on the noise cancellation of the ANC system since it fundamentally relies on common-mode noise cancellation. The degree of noise coherence between the error and reference sensor can be quantified by the coherence function,

$$\gamma^2(f) = \frac{|S_{x,y}(f)|^2}{S_x(f)S_y(f)}, \tag{12}$$

where $S_x(f)$ and $S_y(f)$ are the power spectral densities of the error and noise reference signals and $S_{x,y}(f)$ is the cross power spectral density. The coherence function takes the range

$$0 \le \gamma^2(f) \le 1, \tag{13}$$

where a zero value of coherence implies no correlation between the signals and a value of one implies perfect signal correlation. Real-time estimation of the noise coherence between the noise reference and the error sensors can be used to determine the optimal placement of the noise reference magnetometer relative to the error

magnetometer. The theoretical maximum cancellation of the noise for a given frequency band is given by[34]

$$\alpha(f) = -10\log_{10}\left(1-\gamma^2(f)\right)[\mathrm{dB}]. \quad (14)$$

Active noise control systems applied to cancel the acoustic noise can inadvertently suffer from crosstalk, which occur as a result of the sound generated by the noise canceling speaker propagating and reaching the noise reference microphone. Crosstalk can also occur when attempting to cancel the magnetic field noise if the magnetic field produced by the coils is sensed by the noise reference magnetometer (which is located at a finite distance from the coils). If such fields are strong, they can inadvertently introduce a feedback loop in the ANC system rendering it unstable. One solution is to place the noise reference sensor further away from the coils. However, this comes at the expense of reducing the noise coherence between the reference and error magnetometers.[33] An alternative strategy to mitigate field crosstalk is to use coil geometries that have a one-sided flux pattern which keeps the generated anti-noise field within the inner coil structure where the error sensor resides. This can be achieved through the Halbach-type electromagnet architecture.[35,36] Finally, the noise floor of the in-loop error and noise reference sensors will ultimately impose an upper limit on the noise suppression of the environmental field.

The FxLMS algorithm used in this work is by far the most common approach deployed in active noise control. However, there exists an extensive family of alternative adaptive algorithms that possess a varying degree of capabilities ranging from the speed of convergence to the value of steady state error and computational complexity.[20,37] Depending on the conditions for ANC, a different adaptive algorithm could be employed to enable better performance, e.g., greater noise suppression at the expense of increased hardware and processing requirements. This also applies to the secondary path modeling stage.

V. CONCLUSIONS

We have shown that active noise control is an effective technique for broadband magnetic field noise cancellation. It requires minimal hands on approach to tuning for optimal performance and is flexible for deployment across different hardware architectures. Moreover, in situations where the signals of interest are much smaller than the ambient noise, active noise control implementation can be used to increase the signal to noise ratio by increasing the resolution of the measurement via a reduced input range over the same number of bits. Finally, for highly sensitive devices such as optically pumped magnetometers, where the intrinsic device sensitivity strongly depends on the ambient field noise, an active noise control system can be used to enable highly sensitive operation in magnetically unshielded environments. The gradiometric field measurement approach would especially benefit in this situation as it is often deployed in unshielded environments.

ACKNOWLEDGMENTS

This work was supported by the UK Quantum Technology Hub in Sensing and Timing, funded by the Engineering and Physical Sciences Research Council (EPSRC) (Grant No. EP/T001046/1), the QuantERA grant C'MON-QSENS! by EPSRC (Grant No. EP/T027126/1), the Nottingham Impact Accelerator/EPSRC Impact Acceleration Account (IAA), and Dstl via the Defence and Security Accelerator (www.gov.uk/dasa). We thank Andrew Stuart for electronic engineering support and Yonina Eldar for reading the manuscript.

AUTHOR DECLARATIONS

Conflict of Interest

The authors declare no conflicts to disclose.

DATA AVAILABILITY

The data that support the findings of this study are available from the corresponding authors upon reasonable request.

REFERENCES

[1]R. Fenici, D. Brisinda, and A. M. Meloni, "Clinical application of magnetocardiography," Expert Rev. Mol. Diagn. **5**(3), 291–313 (2005).
[2]Y. Hu, G. Z. Iwata, M. Mohammadi, E. V. Silletta, A. Wickenbrock, J. W. Blanchard, D. Budker, and A. Jerschow, "Sensitive magnetometry reveals inhomogeneities in charge storage and weak transient internal currents in Li-ion cells," Proc. Natl. Acad. Sci. U. S. A. **117**(20), 10667–10672 (2020).
[3]A. Jaufenthaler, P. Schier, T. Middelmann, M. Liebl, F. Wiekhorst, and D. Baumgarten, "Quantitative 2D magnetorelaxometry imaging of magnetic nanoparticles using optically pumped magnetometers," Sensors **20**(3), 753 (2020).
[4]J. W. Blanchard, D. Budker, and A. Trabesinger, "Lower than low: Perspectives on zero-to-ultralow-field nuclear magnetic resonance," J. Magn. Reson. **323**, 106886 (2021).
[5]E. Boto, N. Holmes, J. Leggett, G. Roberts, V. Shah, S. S. Meyer, L. D. Muñoz, K. J. Mullinger, T. M. Tierney, S. Bestmann, G. R. Barnes, R. Bowtell, and M. J. Brookes, "Moving magnetoencephalography towards real world applications with a wearable system," Nature **555**, 657 (2018).
[6]D. Budker and D. F. Jackson Kimball, *Optical Magnetometry* (Cambridge University Press, Cambridge, 2013), ISBN: 9781107010352.
[7]A. Grosz, M. J. Haji-Sheikh, and S. C. Mukhopadhyay, *High Sensitivity Magnetometers* (Springer, 2017), ISBN: 9783319340708.
[8]M. E. Limes, E. L. Foley, T. W. Kornack, S. Caliga, S. McBride, A. Braun, W. Lee, V. G. Lucivero, and M. V. Romalis, "Portable magnetometry for detection of biomagnetism in ambient environments," Phys. Rev. Appl. **14**, 011002 (2020).
[9]G. Oelsner, R. IJsselsteijn, T. Scholtes, A. Krüger, V. Schultze, G. Seyffert, G. Werner, M. Jäger, A. Chwala, and R. Stolz, "Integrated optically pumped magnetometer for measurements within Earth's magnetic field," arXiv:2008.01570 (2020).
[10]R. Zhang, R. Mhaskar, K. Smith, and M. Prouty, "Portable intrinsic gradiometer for ultrasensitive detection of magnetic gradient in unshielded environment," Appl. Phys. Lett. **116**, 143501 (2020).
[11]D. Platzek, H. Nowak, F. Giessler, J. Röther, and M. Eiselt, "Active shielding to reduce low frequency disturbances in direct current near biomagnetic measurements," Rev. Sci. Instrum. **70**, 2465 (1999).
[12]R. Zhang, Y. Ding, Y. Yang, Z. Zheng, J. Chen, X. Peng, T. Wu, and H. Guo, "Active magnetic-field stabilization with atomic magnetometer," Sensors **20**(15), 4241 (2020).
[13]R. Zhang, W. Xiao, Y. Ding, Y. Feng, X. Peng, L. Shen, C. Sun, T. Wu, Y. Wu, Y. Yang, Z. Zheng, X. Zhang, J. Chen, and H. Guo, "Recording brain activities in unshielded Earth's field with optically pumped atomic magnetometers," Sci. Adv. **6**, eaba8792 (2020).
[14]B. Merkel, K. Thirumalai, J. E. Tarlton, V. M. Schäfer, C. J. Ballance, T. P. Harty, and D. M. Lucas, "Magnetic field stabilization system for atomic physics experiments," Rev. Sci. Instrum. **90**, 044702 (2019).
[15]K. Xiao, L. Wang, J. Guo, M. Zhu, X. Zhao, X. Sun, C. Ye, and X. Zhou, "Quieting an environmental magnetic field without shielding," Rev. Sci. Instrum. **91**, 085107 (2020).

[16]S. M. Kuo, I. Panahi, K. M. Chung, T. Horner, M. Nadeski, and J. Chyan, "Design of active noise control systems with the TMS320 family," **1996**, 27–37; available at Texas Instruments, http://www.ti.com/lit/pdf/spra042.
[17]S. M. Kuo, S. Mitra, and W. Gan, "Active noise control system for headphone applications," IEEE Trans. Control Syst. Technol. **14**(2), 331 (2006).
[18]J. C. Driggers, M. Evans, K. Pepper, and R. Adhikari, "Active noise cancellation in a suspended interferometer," Rev. Sci. Instrum. **83**, 024501 (2012).
[19]K. Chen, C. Chang, and S. M. Kuo, "Active noise control in a duct to cancel broadband noise," IOP Conf. Ser.: Mater. Sci. Eng. **237**, 012015 (2017).
[20]S. M. Kuo and D. R. Morgan, "Active noise control: A tutorial review," Proc. IEEE **87**(6), 943 (1999).
[21]V. Tiporlini and K. Alameh, "Optical magnetometer employing adaptive noise cancellation for unshielded magnetocardiography," Univers. J. Biomed. Eng. **1**(1), 16–21 (2013).
[22]N. V. Thakor and Y. S. Zhu, "Applications of adaptive filtering to ECG analysis: Noise cancellation and arrhythmia detection," IEEE Trans. Biomed. Eng. **38**(8), 785 (1991).
[23]B. Widrow, J. R. Glover, J. M. McCool, J. Kaunitz, C. S. Williams, R. H. Hearn, J. R. Zeidler, E. Dong, Jr., and R. C. Goodlin, "Adaptive noise cancelling: Principles and applications," Proc. IEEE **63**(12), 1692 (1975).
[24]J. C. Allred, R. N. Lyman, T. W. Kornack, and M. V. Romalis, "High-sensitivity atomic magnetometer unaffected by spin-exchange relaxation," Phys. Rev. Lett. **89**, 130801 (2002).
[25]D. Sheng, A. R. Perry, S. P. Krzyzewski, S. Geller, J. Kitching, and S. Knappe, "A microfabricated optically-pumped magnetic gradiometer," Appl. Phys. Lett. **110**, 031106 (2017).
[26]G. Bevilacqua, V. Biancalana, Y. Dancheva, and A. Vigilante, "Self-adaptive loop for external-disturbance reduction in a differential measurement setup," Phys. Rev. Appl. **11**, 014029 (2019).
[27]D. Manolakis and J. G. Proakis, *Digital Signal Processing: Principles, Algorithms, and Applications*, 4th ed. (Pearson, 2006), ISBN: 978-0131873742.
[28]W. Kester, *Mixed-Signal Design Seminar* (Analog Devices, 1991), ISBN: 0-916550-08-7.
[29]S. L. Netto, P. S. R. Diniz, and P. Agathoklis, "Adaptive IIR filtering algorithms for system identification: A general framework," IEEE Trans. Educ. **38**(1), 54 (1995).
[30]LabVIEW Digital Filter Design Toolkit, LabVIEW.
[31]See https://quspin.com/products-qzfm/ for QZFM Gen-2 Technical Specifications.
[32]I. T. Ardekani and W. Abdulla, "FxLMS-based active noise control: A quick review," in APSIPA, ASC, 2011.
[33]P. J. M. Wöltgens and R. H. Koch, "Magnetic background noise cancellation in real-world environments," Rev. Sci. Instrum. **71**, 1529 (2000).
[34]S. M. Kuo and D. R. Morgan, *Active Noise Control Systems Algorithms and DSP Implementations* (John Wiley & Sons, New York, NY, 1996).
[35]K. Halbach, "Design of permanent multipole magnets with oriented rare earth cobalt material," Nucl. Instrum. Methods **169**(1), 1–10 (1980).
[36]B. Shen, L. Fu, J. Geng, X. Zhang, H. Zhang, Q. Dong, C. Li, J. Li, and T. A. Coombs, "Design and simulation of superconducting Lorentz force electrical impedance tomography (LFEIT)," Physica C **524**, 5–12 (2016).
[37]R. Martinek, R. Kahankova, J. Nedoma, M. Fajkus, and M. Skacel, "Comparison of the LMS, NLMS, RLS, and QR-RLS algorithms for vehicle noise suppression," in ICCMS 2018: Proceedings of the 10th International Conference on Computer Modeling and Simulation, 2018.